Protein Precipitation: Effects of Mixing on Protein Solubility

Harish V. Iyer and Todd M. Przybycien
Bioseparations Research Center, Dept. of Chemical Engineering, Rensselaer Polytechnic Institute, Troy, NY 12180

Mixing effects in protein precipitation processes are very poorly understood. They impact apparent protein solubility, protein structure in precipitates, particle size, morphology and recoverable activity. In this work, a model is proposed to describe the impact of mixing on protein solubility in precipitation processes. A series of semibatch-mode precipitation experiments were performed using bovine liver catalase and ammonium sulfate to test model predictions. The process variables studied include initial protein supersaturation, agitation rate, and rate of addition of salt solution to the initial protein solution. The mixing model parameters were estimated independently with the aid of a series-parallel dye reaction. The results showed good agreement between model and experiment. The initial protein supersaturation was the most important variable at the 1-L scale. The influence of mixing on recoverable activity was also examined. Scale-up guidelines are suggested based on model simulations and experimental results.

Introduction

Salt-induced protein precipitation operations are ubiquitous in recovery and purification trains for protein products. Hofmeister (1887, 1890) first described the use of neutral salts to precipitate protein. Salting-out processes, with ammonium sulfate in particular, have been in wide use since that time; Englard and Seifter (1990) have estimated that up to 80% of published protein purification protocols involve at least one salting-out step. The use of precipitation ranges from primary isolation procedures (Nakayama et al., 1987; Michaels, 1990) for the separation of product protein from cell debris in recombinant cell cultures, to finishing operations (Bell et al., 1983; Paul and Rosas, 1990) for the production of solids prior to drying and formulation. Process scale precipitations which are used to reduce processing volumes and concentrate desired product, usually result in the formation of amorphous precipitates rather than crystals. Fractionation is also possible by semiselective precipitation based on the relative solubilities of proteins (Niktari et al., 1990; Nelson and Glatz, 1985; Fisher et al., 1986; Rothstein, 1990).

Despite the widespread use and apparent maturity of salting-out processes, the salt and protein physical properties and solution conditions governing protein solubility are not well understood. The difficulty in quantifying protein solubility in practice arises from the fact that in general, "protein precipitation is not a thermodynamically reversible process, that is, the final state depends on the specific process (path) employed" (Rothstein, 1991). The Cohn equation which is commonly used to describe the solubility of proteins in salt solutions, gives solubility, P^*, as a function of salt concentration, S, as (Cohn, 1943):

$$\ln P^* = \beta - K_S S \tag{1}$$

where β is a constant which depends on pH and temperature and K_S is the salting-out constant which depends on protein and salt physical properties (Melander and Horvath, 1977). However, due to the rapidity of the initial protein desolvation reaction and kinetic irreversibility arising from subsequent aggregation reactions, both K_S and β are found to vary with mixing conditions as well. Foster and coworkers (1976) characterized the apparent solubility of a crude fumarase preparation under a variety of mixing conditions; small batch precipitation experiments gave apparent solubilities that differed by several orders of magnitude from those observed in large continuous precipitations in stirred tank reactors at equivalent salt and protein concentrations. Thus, the apparent protein solubility will depend on the distribution of microenvironments, or mixing conditions, within the precipitation reactor.

Correspondence concerning this article should be addressed to T. M. Przybycien.

Overprecipitation occurs when the initial protein concentration exceeds the protein solubility at the initial salt concentration; imperfect mixing leads to the transient contact of regions of locally high salt and high protein concentrations. Under these conditions precipitation is essentially irreversible. Local solubilities will determine the local supersaturation levels, impacting precipitate particle-size distributions and morphology via nucleation and primary particle formation phenomena (Przybycien and Bailey, 1989b; Chan et al., 1986; Nelson and Glatz, 1985; Åslund and Rasmuson, 1992), recoverable activity via denaturing exposure to transiently high salt concentrations (Przybycien and Bailey, 1989a, 1991) and product purity via variations in local differential solubilities. Although it is not necessary that overprecipitation be avoided, the ability to predict and possibly control its extent is desirable because of these relationships with particle size and morphology, recoverable activity and purity.

The impact of mixing phenomena on protein solubility in protein precipitation has not been rigorously tested previously. However, the reactive precipitation of inorganic salts has been extensively treated in the literature (Pohorecki and Baldyga, 1983, 1988; Randolph and Larson, 1971; Garside and Tavare, 1985; Fitchett and Tarbell, 1990; Marcant and David, 1991; Tavare and Patwardhan, 1992). While these studies have suggested a framework for modeling protein precipitation, scale-up parameters based on the results obtained from precipitation of inorganic materials do not present an entirely accurate view of protein precipitation, as proteins may undergo reversible or irreversible conformational changes (Przybycien and Bailey, 1989b) and become kinetically trapped in the course of a precipitation. Inorganic salt precipitations are often reversible and, hence, solubility is only transiently affected by contacting conditions.

In this work, we present the impact of process variables including initial protein supersaturation, salt solution addition rate and agitation rate on apparent protein solubility in semi-batch precipitations at the 1-L scale. The model protein was bovine liver catalase, a well characterized heme protein with a well-defined three-dimensional structure (Reid et al., 1981) and an easily assayable activity. The model salt was ammonium sulfate, one of the most commonly used protein precipitants (Bell et al., 1983; Scopes, 1982). We have also proposed a mixing model that provides qualitative predictions of apparent protein solubilities as a function of process variables.

Theoretical Development

Mixing model development

The extent of mixing in a reactor is characterized by both the macromixing and the micromixing. Macromixing is the dissipation of bulk fluid elements in the reactor. The extent of macromixing depends upon the rate of agitation, the geometric dimensions of the reactor, the rate of addition of precipitant into the reactor and the feed geometry, subsurface or otherwise (Pohorecki and Baldyga, 1983). Macromixing is thought to occur through convective or flow-dominated processes whereby bulk fluid elements are deformed until their scale of segregation, the length over which the fluid elements are homogeneous, is comparable to the Kolmogoroff microscale, λ_K (Drake, 1972):

$$\lambda_K = \left(\frac{\nu^3}{\epsilon}\right)^{1/4} \tag{2}$$

where ν is the kinematic viscosity of the fluid in the system and ϵ is the power input per unit mass to the reactor. Mixing continues to occur below the scale of λ_K through the process of molecular diffusion and is termed micromixing (Bourne, 1983; Danckwerts, 1953). The intensity of micromixing is an indication of the extent of molecular homogeneity in a given reactor.

The model we have developed to describe the contact between protein and precipitant in the reactor is based on the spectral interpretation of mixing in an isotropic homogeneous turbulent field proposed by Pohorecki and Baldyga (1983). As shown in Figure 1, the reactor volume is assumed to be comprised of a completely segregated zone and a molecular dissipation zone. In semi-batch operation, the reactant solution fed to the reactor and the solution that is present in the reactor initially are assumed to form two totally segregated zones. These segregated volumes undergo deformation and breakage due to macromixing. The breakup of these volumes into smaller eddies is assumed to take place through a first-order dissipation process (Rosensweig, 1964). The persistence of the segregated zones is characterized by:

$$\frac{dV_c(t)}{dt} = -k_{ms}V_c(t) + F_c(t) \tag{3}$$

where V_c is the segregated volume and F_c is the volumetric feed rate of the solution of component C. The dependence of the macromixing rate constant k_{ms} on the impeller agitation rate, the power input to the reactor per unit mass and the reactor geometry was obtained through dimensional analysis by Pohorecki and Baldyga (1983). Since we have a variable-volume system, k_{ms} will vary with time. However, since the changes are small, average values of the parameter are assumed to be sufficient.

The zone in which the eddies have been reduced to the Kolmogoroff scale is the molecular dissipation zone. All eddies whose length scale is below λ_K are called *points* (Danckwerts, 1953); reactants meet in this zone and react. Micromixing or molecular level diffusion processes in this zone are driven by the concentration gradients between a point and its surroundings, which comprises the remaining points (Costa and Trevissoi, 1972). A mass balance on the ith point for a generic component C is given by:

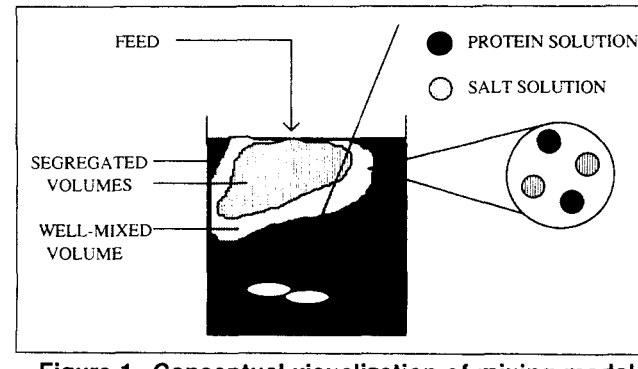

Figure 1. Conceptual visualization of mixing model.

$$\frac{dC_i(t-\tau)}{dt} = k_{md}[\overline{C}(t) - C_i(t-\tau)] - \Re_{c_i}(t-\tau) \quad (4)$$

where C_i is the concentration of C in the ith point, k_{md} is a lumped parameter that describes the rate of mass transfer between a point and its surroundings, $\overline{C}(t)$ is the volume average concentration of the species over all the points in the molecularly mixed zone and $\Re_{c_i}(t-\tau)$ is the rate of consumption of C by reaction within the ith point. In Eq. 4, t is the elapsed time in the precipitation and τ is the time at which the ith point forms; $t-\tau$ is the age of the ith point. Equation 4 is generalized, allowing for the continuous formation of several different types of points. The micromixing constant k_{md} depends upon the Schmidt, Reynolds and power numbers as well as the geometry of the vessel. This relationship, obtained by dimensional analysis, has also been given by Pohorecki and Baldyga (1983). Since k_{md} depends logarithmically on the Schmidt number, its variation with respect to salt and protein species is small despite large differences in the diffusion coefficients.

We postulate the formation of two types of points in the micromixed zone for our two component semi-batch system. Type 1 points are formed by the dissipation of the bulk solution present in the reactor at time $t=0$. Type 2 points are formed continuously by the disintegration of the bulk feed stream into the molecularly mixed zone. These points may be distinguished by the initial conditions used in Eq. 4.

For closure, we must determine the surrounding or average concentration of each component in the mixed zone for Eq. 4. $\overline{C}(t)$ may be obtained via a mass balance:

$$-\frac{d}{dt}[\overline{C}(t)V_m(t)] = \sum_{i=1}^{2}\left(\int_0^t \frac{dV_i(\tau)}{d\tau}\Re_{c_i}(t-\tau)d\tau\right) - C_b k_{ms} V_c(t) \quad (5)$$

where V_m is the volume of the molecularly mixed zone, V_i is the total volume of type i points, V_c is the bulk solution volume of component C and C_b is the concentration of C within V_c. The integral in the above equation describes the removal or formation of C due to reaction in either type 1 or 2 points, accounting for the continuous formation of these points as the segregated zones are dissipated. The term $C_b k_{ms} V_c(t)$ is the influx of C from the segregated zones. Equation 5 assumes that $\overline{C}(t)$ is well represented by the volume average concentration of C over all types of points. The total volume of type 1 points is given by:

$$\frac{dV_1(t)}{dt} = k_{ms}V_p(t) \text{ with } V_1(0)=0 \quad (6)$$

where V_p is the volume of the solution present initially in the reactor. Likewise, the total volume of type 2 points is given by:

$$\frac{dV_2(t)}{dt} = k_{ms}V_s(t) \text{ with } V_2(0)=0 \quad (7)$$

where V_s represents the segregated volume of the solution fed to the system.

Application of mixing model to protein precipitation

In the semibatch precipitation process we have studied, the salt solution is added to the protein solution present initially in the reactor. The volume of the protein solution present originally in the reactor is:

$$V_p(0) = V_{po} \quad (8)$$

and since there is no salt initially in the semibatch system:

$$V_s(0) = 0. \quad (9)$$

The feed rate of salt solution, F_s, is given as:

$$F_S(t) = \begin{cases} F_S & 0 \le t \le t_f \\ 0 & t > t_f \end{cases}. \quad (10)$$

Based on our model, the dissipation of the segregated salt and protein zones is assumed to create two types of points: those formed from the protein solution are labeled type 1 points, and those formed from the dissipation of the salt solution are labeled type 2 points. Species concentrations in both types of points are determined through mass balances via Eq. 4. Type 1 points start with protein at its initial concentration:

$$P_1(0) = P_o \text{ and } S_1(0) = 0 \quad (11)$$

and type 2 points are formed with salt at its feed concentration:

$$P_2(0) = 0 \text{ and } S_2(0) = S_o. \quad (12)$$

Finally, since there is no micromixed volume present initially:

$$\overline{P}(0)V_m(0) = \overline{S}(0)V_m(0) = 0. \quad (13)$$

When the protein concentration in a given point exceeds the solubility, as determined by Eq. 1, precipitation occurs. Protein precipitation may be represented by a series of reactions consisting of protein dehydration:

$$P\cdot(x+y+z)H_2O \xrightarrow{k_r} P\cdot xH_2O + (y+z)H_2O \quad (14)$$

aggregation of dehydrated protein:

$$P\cdot xH_2O \rightarrow \text{aggregates} \quad (15)$$

and salt ion hydration:

$$A_mB_n + (y+z)H_2O \rightarrow mA^{n+}\cdot yH_2O + nB^{m-}\cdot zH_2O \quad (16)$$

where A^{n+} and B^{m-} are the salt cation and anion respectively. This mechanistic outline is consistent with Arakawa and Timasheff's (1982, 1987) view of precipitation as the preferential interaction of solvent (water) molecules with salt ions, leading to a destabilization of the protein in solution. A complementary view is that salt ion hydration leads to an increase in the solution surface tension which is unfavorable with respect to the hydration of hydrophobic patches on the protein surface; the protein aggregates to minimize the total solvent-exposed hy-

drophobic surface area (Sinanoglu and Abdulnur, 1965; Halicioglu and Sinanoglu, 1969; Melander and Horvath, 1977). Note also that the protein desolvation represented in Eq. 14 may be accompanied by a conformational change (Przybycien and Bailey, 1991). The rapidity of the protein desolvation is responsible for the mixing control of protein solubility.

As we are concerned here with protein solubility, we need only focus on the protein dehydration reaction (Eq. 14) to develop a protein consumption term for the mass balance in Eq. 4. The protein desolvation rate is modeled as:

$$\Re(P_i, P^*) = k_r(P_i - P^*(S_i))H[P_i - P^*(S_i)]. \quad (17)$$

where k_r is the rate constant associated with reaction 14, $P^*(S_i)$ is the thermodynamic solubility at salt concentration S_i, from Eq. 1 and $H(x)$ is the Heaviside unit step function. We have assumed that the desolvation reaction is first-order in protein supersaturation. The supersaturation is an expression of the reduction in free water available for protein hydration; the assumption of a first-order dependence on supersaturation represents, in a sense, mass-action kinetics with respect to free water. The Heaviside function accounts for the kinetic irreversibility of desolvation arising from the subsequent aggregation step described in reaction 15. Most of the protein will be trapped in the interior of aggregate particles and will not remain in equilibrium with solvated protein. The inclusion of the Heaviside function results in a deterministic model; the nontrivial steady-state solution for protein solubility may be obtained only by simulating the entire transient period. Since we assume salt is not consumed by the desolvation reaction:

$$\Re(S_i) = 0. \quad (18)$$

Thus, the concentration of salt in the points and the environment varies only due to mass transfer and is controlled by the extent of micromixing in the reactor.

The cumulative mass of desolvated protein at time t, $M_p(t)$, can be computed as an integral of the total amount reacted in all the points formed over the time interval [0, t]:

$$\frac{dM_p(t)}{dt} = \sum_{i=1}^{2} \left(\int_0^t \frac{dV_i(t-\tau)}{d\tau} \Re_{c_i}(\tau) d\tau \right) \quad \text{with } M_p(0) = 0. \quad (19)$$

Alternatively, the ultimate total amount of protein precipitated can be obtained by an overall mass balance on the protein in solution:

$$\lim_{t\to\infty} M_p(t) = P_o V_{po} - \lim_{t\to\infty} \overline{P(t)} V_m(t). \quad (20)$$

This expression can be used as a final material balance check on the model equations. Again, due to Eq. 17, the steady-state mass of precipitate is deterministic.

To reduce the stiffness of the system of equations, the model variables were nondimensionalized. The protein concentration was nondimensionalized using the ultimate thermodynamic solubility of the protein solution at the final salt concentration, $\lim_{t\to\infty} P^*(\bar{S}(t)) = P^*(\infty)$. The scaling parameters for the salt concentration, all volumes and time were K_s, V_{total} and the micromixing rate constant k_{md}, respectively.

Application of mixing model to series-parallel reaction for parameter estimation

The parameters k_{ms} and k_{md} in the mixing model were determined experimentally using a series-parallel dye reaction (Bourne et al., 1981):

$$A + B \xrightarrow{k_1} R \quad (21)$$

$$B + R \xrightarrow{k_2} S \quad (22)$$

In the dye reaction, A is 1-naphthol, B is diazotized sulfanilic acid, R is 4-(4′-sulphophenylazo)-1-naphthol which is the monoazo dyestuff and S is 2,4-(4′-sulphophenylazo)-1-naphthol which is the bisazo dyestuff. The presence of a trace amount of a third dye product was ignored as reaction rate data for this product were not available for simulation (Wenger et al., 1992).

The dye reactions were done in the same reactor in which the precipitation experiments were carried out. The volumetric ratio of A to B was 19:1. The experiments were done in batch mode, with the reactants having an initial molar ratio of 1:1. A solution of 1-naphthol was present initially in the reactor and diazotized sulfanilic acid was added to this system. The reaction was assumed to go to completion; this occurred within a few minutes after the addition of the second reagent. The reactor contents were analyzed via UV-Vis spectroscopy to determine concentrations of the mono-azo and bis-azo dyestuffs. From this measurement, the selectivity, $\mathbb{S}$, of the reaction under the mixing conditions employed could be computed as:

$$\mathbb{S} = \lim_{t\to\infty} \frac{2S(t)}{2S(t) + R(t)}. \quad (23)$$

The rate constants k_{ms} and k_{md} were estimated by applying the mixing model to the dye reaction system and matching the simulation selectivities with the experimental values.

Again, we hypothesized the existence of two types of points. Type 1 and type 2 points were formed from the dissipation of A and B respectively. The reaction rates in a point i can be written as:

$$\Re_{A_i} = -k_1 A_i B_i \quad (24)$$

$$\Re_{B_i} = -k_1 A_i B_i - k_2 B_i R_i \quad (25)$$

$$\Re_{R_i} = k_1 A_i B_i - k_2 B_i R_i \quad (26)$$

$$\Re_{S_i} = k_2 B_i R_i. \quad (27)$$

The values of the reaction rate constants were $k_1 = 7.3 \times 10^6$ L/(mol·s) and $k_2 = 3.5 \times 10^3$ L/(mol·s) (Bourne et al., 1981).

Numerical solution of mixing model equations

The protein solubility term in the reaction part of the mixing equations has an exponential dependence via the Cohn equa-

tion, causing the equations to be stiff. The equations were solved numerically by Gear's method using the Differential and Algebraic System Solver (DASSL, Petzold, 1983). The initial condition $V_m(0) = 0$ causes an indeterminacy in the numerical solution. Therefore, a value of 10^{-12} was assigned to V_m/V_{total} to start the numerical integration.

Materials and Methods

Materials

Catalase was used as a model protein and was obtained as a crude mixture from Sigma, St. Louis, MO (catalog #C-10, lot 81H7146). An isoelectric focusing gel run on the sample showed it to be a mixture of proteins. The purity of this mixture was assessed to be approximately 7-10% based on activity assays. A more homogeneous catalase preparation was also obtained from Sigma (catalog #C-100, lot 11H7305) for thermodynamic solubility determinations. The native, active protein is a tetramer with four identical subunits, each of molecular weight 57,000 Da and is slightly ellipsoidal with an average radius of 40 Å (Ried et al., 1981). The isoelectric point is 6.7 (Righetti and Caravaggio, 1976). All experiments were carried out in 0.05-M phosphate buffer, pH 7.0, where the solubility of catalase was close to its minimum. The precipitant used in the experiments, $(NH_4)_2SO_4$, and the buffer salts for the dye reaction experiments were also obtained from Sigma. The 1-naphthol and the sulfanilic acid used in the dye experiments for mixing parameter estimation were obtained from Lancaster Chemicals, Windham, NH. Distilled, deionized water was used throughout. All experiments were carried out at 25 ± 1 °C unless otherwise noted.

Determination of Cohn solubility parameters

The thermodynamic solubility curve of catalase was determined as a function of $(NH_4)_2SO_4$ concentration to provide estimates for the Cohn parameters, K_S and β. The thermodynamic solubility of catalase as a function of ammonium sulfate concentration was determined via the dissolution of solid phase protein over a period of 12-24 h. The solid protein dissolves until the solution is saturated; in this way, *the solution is never supersaturated and overprecipitation does not occur.*

Initially, 200-300 mg of solid catalase was added to a 15-mL Corning centrifuge tube. A 10-mL aliquot of an ammonium sulfate solution of known concentration was slowly pipetted into the centrifuge tube. The centrifuge tube was then capped and put on a heavy duty rotator at very low speeds and a shallow angle to ensure gentle mixing without foaming. The entire apparatus was left overnight in a constant temperature room maintained at 25°C to come to equilibrium. The tubes were then centrifuged and the supernatant analyzed for protein concentration using the Coomassie Blue dye-binding assay obtained from BioRad (Sedmak and Grossberg, 1977). Provided some solid protein remained undissolved, this concentration was the solubility of the protein at the given salt concentration.

Precipitation reactor

A 1-L water-jacketed glass vessel obtained from Kontes, Vineland, NJ was used to carry out the precipitations in both batch and semi-batch modes. Figure 2 shows a schematic of the reactor setup. An instrumented agitator motor, Lightnin model TSM2510 was used in conjunction with a three-blade marine type impeller (see Figure 2 inset) obtained from Fisher for mixing. A Masterflex computerized peristaltic pump obtained from the Cole-Parmer Instrument Company, Chicago, IL was used to pump the salt solution into the reactor. The temperature in the reactor was maintained at 25°C with a circulating water bath. The time involved for the precipitation runs varied from about 15 to 80 min. Even for shorter precipitation times, continued mixing over several hours did not change the apparent protein solubility.

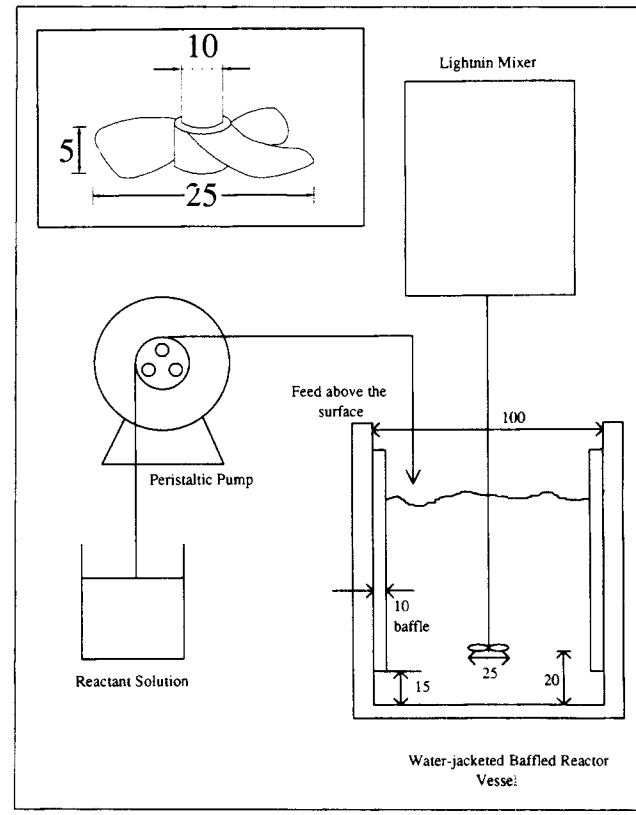

Figure 2. Apparatus for batch and semibatch precipitation experiments.

Inset details 3-blade marine impeller used. All dimensions in mm.

Mixing characterization via dye reaction experiments

The diazotized sulfanilic acid was prepared using the method of Wistar et al. (1941). For the mixing characterization experiments, the volumes of 1-naphthol and diazotized sulfanilic acid used were 784.0 and 16.0 mL, respectively. The final concentrations of each of the solutions was 1.25×10^{-5} M. Batch addition experiments were performed in triplicate at impeller speeds of 60, 180 and 540 rpm. Slower reagent addition rates were not used as the diazotized sulfanilic acid decomposed in short periods of time. The optical absorbances of the dye reaction products were determined at three different wavelengths, 400, 500 and 600 nm. The total absorbance, A_λ, at wavelength λ, is given by Beer-Lambert's law as:

$$A_\lambda = \epsilon_R(\lambda) Rl + \epsilon_S(\lambda) Sl \tag{28}$$

Table 1. Extinction Coefficients of Mono and Diazo Dyestuffs

Wavelength (nm)	ϵ_R (m^2/mol)	ϵ_S (m^2/mol)
400	460	750
500	3,100	1,958
600	100	1,375

where $\epsilon_R(\lambda)$ and $\epsilon_S(\lambda)$ are the extinction coefficients of R and S at λ which are listed in Table 1 (Bourne et al., 1981) and l is the path length which is equal to 1 cm. A least-squares fit was done to determine the values of R and S from the multiple wavelength absorbance measurements. The mass balance for the dye reaction system closed to within about 97% on average. This is consistent with the observations reported by Wenger and coworkers (1992).

Precipitation experimental design and procedure

The precipitation experiments were done by varying three factors that were considered the most important in the process: the impeller agitation rate, rate of addition of salt solution and the initial concentration of the protein solution. An experimental design was followed to plan the experiments and analyze the resulting data to obtain statistically meaningful conclusions. The statistical analysis is based on linear interpolation, but since the salt feed rate and impeller agitation rate were varied geometrically, common logarithms were used to obtain a linear scale for both of these parameters. The factors were assigned labels X_1 for the $\log_{10}$ (impeller agitation rate in rpm), X_2 for the initial protein concentration in mg/mL and X_3 for the $\log_{10}$ (salt addition rate in mL/min) in the following analysis. High, medium and low values were chosen for each of the variables and were assigned values +1, 0 and −1. The measured variable was the final apparent solubility, represented by Y. The (0, 0, 0) or midpoint experiments were performed in triplicate in order to obtain an estimate of the experimental error. Main effects as well as two-factor and three-factor interaction effects were computed based on the experimental results. The computation of the interaction effects does not require the results obtained for the midpoint experiments; thus, the reliability of the statistical analysis can be tested at the midpoint. This analysis enabled us to estimate values for solubility, within the parameter limits, in regimes where no experiments were performed. The high and low parameter values were chosen as wide apart as possible so that final solubilities could be predicted over a wider range of mixing conditions. A more detailed explanation of the analysis is given by Doehlert (1989).

Preparation of precipitate samples for solubility and activity assay

Precipitate samples for the activity assay were obtained by centrifuging samples for 15 min at 15,000 rpm at 25°C. The sediment was resuspended in phosphate buffer. After dissolution by gentle end to end rotation for approximately 30 min, the solution was centrifuged again to remove any residual insoluble material. The final supernatant was assayed for catalase concentration and activity.

Table 2. Selectivities of Batch Addition Dye Reaction Experiments as a Function of Mixing Conditions and Corresponding Mixing Constants from Simulations

rpm	S^*	k_{md}(1/min)	k_{ms}(1/min)
60	0.311 ± 0.042	0.06	0.57
180	0.199 ± 0.017	0.58	2.08
540	0.114 ± 0.015	5.88	5.88

*Mean selectivity ± S.D. of triplicate measurements. Computed as described in materials and methods.

Protein activity assay

An activity assay was used to measure the recoverable activity of the redissolved precipitate. The assay, based on the ability of catalase to decompose hydrogen peroxide into water and oxygen, was done in accordance with the protocol outlined in the Sigma Chemical Company catalog.

Results and Discussion

Dye reaction experiments

The dye reaction experiments were done at three different impeller speeds and the observed selectivities are presented in Table 2. The experimental selectivities were fitted manually with the mixing model to obtain rough estimates for the average mixing rate constants k_{ms} and k_{md}. The model fits were not very sensitive to the values of k_{ms} and k_{md} in the neighborhood of the optimum fit. The values of the fitted constants are shown in Table 2. These were used later to compute theoretical apparent protein solubilities.

Reversible solubility experiments

The data from the thermodynamic solubility experiments described above are shown in Figure 3. These solubility data exhibit the typical log-linear salt concentration dependence described by the Cohn equation (Eq. 1). The thermodynamic solubility relationship for the crude catalase mixture was ob-

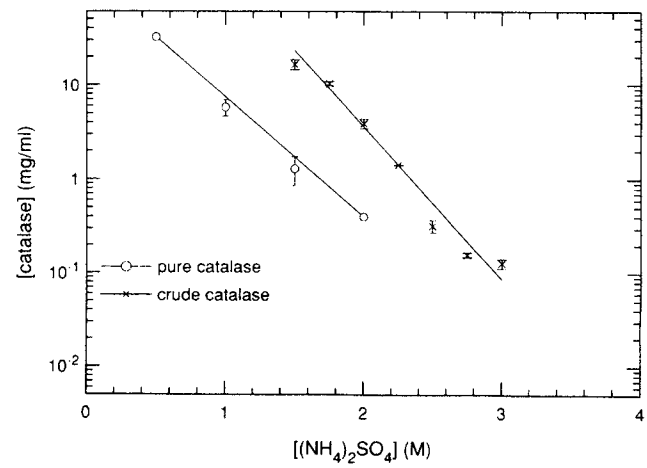

Figure 3. Thermodynamic solubility of crude and pure bovine liver catalase preparations in ammonium sulfate.

Error bars represent ± S.D. of the mean of triplicate measurements.

tained by performing a weighted least-squares fit of the data in the salting-out region to the Cohn equation giving:

$$\ln(P^*) = (8.74 \pm 0.13) - (3.73 \pm 0.06)S. \quad (29)$$

The solubility of pure catalase was determined similarly. The data, also shown in Figure 3, were fitted to the Cohn equation giving:

$$\ln(P^*) = (4.94 \pm 0.02) - (2.93 \pm 0.06)S. \quad (30)$$

The values of K_s and β are reported with corresponding estimates of the standard error of the mean.

Precipitation experiments

Experimental Design. The experimental design enabled us to predict the response of the reactor system in terms of the three chosen variables using a very small number of experiments. The various main effects and interactions were obtained from the analysis of the resulting experimental solubilities. The magnitude of the coefficient b_i in the statistical analysis (see Table 4) is a measure of the main effect of a given variable. The statistical analysis showed that the initial protein concentration (X_2) had the dominant effect on apparent solubility (Y). Other effects due to the impeller speed (X_1) and the salt addition rate (X_3) were an order of magnitude lower. The analysis was also able to show the extent of interactions between the parameters through the magnitudes of the b_{ij}. If an interaction b_{ij} is negative, then the effect of increasing X_i and X_j simultaneously on Y is less than the combination of their separate effects. The prediction of the interaction effects was one of the most important motivations for choosing an experimental design. For example, b_{12} is positive and therefore increasing both the impeller speed and initial protein concentration would cause an increase in apparent solubility that was higher than the individual effects. The interaction between impeller speed and salt addition rate was the strongest.

Since the statistical analysis did not use the experiments done at the midpoint, the midpoint data can be used to assess the accuracy of the statistical analysis. The midpoint solubility from the experimental design equation, b_o in Table 4, is equal to the value of solubility at (0, 0, 0). The computed value of b_o, 6.24 mg/mL, agrees closely with the average of the experimental values, 6.11 ± 0.51 mg/mL.

Initial Protein Concentration. The experiments performed using the crude catalase and ammonium sulfate showed a strong dependence of ultimate solubility on mixing effects. The initial protein concentration was found to influence the apparent solubility to the greatest extent (see Table 3). Even solutions whose initial protein concentrations were below the thermodynamic solubility showed precipitation. In our experiments, the concentrations of the protein and salt solutions in contact initially are double their final average concentrations resulting in overprecipitation. The extent of the impact of initial protein concentration is most clearly demonstrated by a comparison of the measured apparent solubilities for initial and protein concentrations of 25 and 4 mg/mL given in Table 3. For the 25-mg/mL initial protein concentration experiments, the apparent solubilities ranged from 8.35 to 12.87 mg/mL; the 4-mg/mL initial protein concentration runs gave apparent solubilities between 1.87 and 2.09 mg/mL. Thus, *mixing effects lead to precipitation even when the initial protein concentration is less than the apparent solubility determined at higher initial concentrations.*

Salt Addition Rate. The salt addition rate did not affect the solubility to as great an extent as the initial protein concentration (see Table 3). Increasing the salt addition rate at a fixed initial protein concentration resulted in a slightly depressed apparent solubility. There are two opposing effects as the salt addition rate increases. At higher feed rates, larger volumes of the highly concentrated segregated salt solution produce a larger number of type 2 points in a given period of time, leading to increased precipitation. At the same time, faster addition of salt solution causes faster dilution of the protein and salt solutions in the well-mixed zone due to higher dissipation rates. This dilution effect reduces the extent of precipitation by reducing the local supersaturation. The overall impact is a balance of the two effects described above. At the 1-L scale, the solubility decreases with an increase in the feed addition rate. The effect of salt addition rate, and hence b_3, is expected to increase when experiments are performed at larger scales due to enhanced persistence of segregated regions.

Impeller Agitation Rate. The impeller speed had the least effect on the ultimate protein solubility (see Table 3). The primary effect of the impeller speed is on the dissipation of the precipitant and protein solutions into the micromixed zones. Therefore, an increase in the impeller speed increases the rate of dissipation and hence dilution of the protein and salt concentrations. This reduces the extent of overprecipitation by reducing the concentration differences quickly. The experimental data show this as a low-level effect. This is likely due to the small scale of our system as the segregation is not extensive even at relatively low impeller speeds; the impeller

Table 3. Comparison of Experimental and Theoretical Analysis for Apparent Protein Solubility and Recoverable Activity

Agitation (rpm)	F (mL/min)	P_o (mg/mL)	Solubility (mg/mL, exp.)	Solubility (mg/mL, theory)	Activity (U/mg)
60	200	25	8.35	9.53	1,112
60	200	4	1.92	1.94	1,003
60	8	25	10.55	9.60	2,079
60	8	4	1.87	1.94	1,530
180	40	14.5	6.11 ± 0.51	6.04	$2,365 \pm 325$
540	200	25	10.17	9.54	2,052
540	200	4	2.09	1.94	1,650
540	8	25	12.87	9.60	2,003
540	8	4	2.07	1.94	630

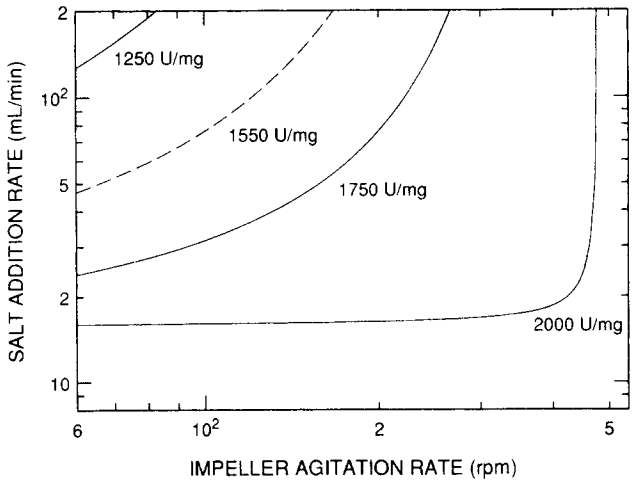

Figure 4. Contour plot of effect of salt addition rate and impeller agitation rate on final protein activity.

Dashed line represents initial protein activity of 1,550 U/mg.

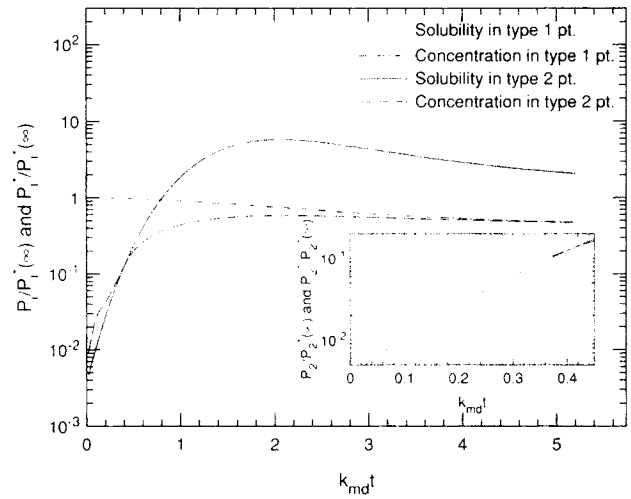

Figure 5. Simulated protein concentration and solubility trajectories for type 1 and type 2 points.

Protein concentration and solubility normalized by the ultimate thermodynamic solubility. Inset details the early time behavior in type 2 points. Parameter values: $P_o/P^*(\infty) = 1.0$, $K_sS_o = 11.19$, $\beta = 8.74$, $F_s/(k_{md}/V_{total} = 0.25$, $k_{ms}/k_{md} = 1.0$, and $k_r/k_{md} = 50.0$.

power inputs ranged from 0.004W/L (60 rpm) to 1.3W/L (540 rpm).

Recoverable Activity. The activity of the resuspended precipitate phase was found to vary considerably with the mixing conditions. The values of the recovered activity ranged from over 2,100 U/mg to below 1,000 U/mg; the starting material had an activity of approximately 1,550 U/mg. Total activity balances for representative precipitate samples yielded activity losses ranging from 18 to 25%. A statistical analysis was also used to determine the effects of mixing on activity. The analysis shows that initial protein concentration and impeller speed have strong positive effects, that is, increases in their values increase the recoverable activity. Figure 4, obtained from the analysis, shows both decreases and increases in the precipitate activity relative to the starting material. Better mixing, either via slower addition or faster agitation, results in higher activity. Two possible reasons can be suggested for these changes in the recoverable activity. First, during the course of a precipitation, a certain amount of fractionation occurs as the solubility of pure catalase is different from the solubility of the overall mixture (see Figure 3). Since the solubility of the pure catalase is lower than the crude preparation, one can expect an enrichment of catalase in the precipitate phase and therefore an enhancement in activity. Second, since there is a decrease in the total overall activity after precipitation, harsh salt conditions in the precipitation reactor may cause partial denaturation of the protein, resulting in a decrease in the activity of the precipitated protein. Quicker addition of salt at lower impeller speeds results in poor mixing in the reactor and exposure of protein to more extreme salt concentrations. Isoelectric focusing gels and preliminary electron paramagnetic resonance spectra of precipitate samples (data not shown) indicate that both enrichment and denaturation occur. Both effects depend on the persistence of bulk salt solution in the reactor and, consequently, the contacting conditions during a salting-out operation. However, experiments done at the midpoint (0, 0, 0) show the maximum recoverable activity (see Table 3). There is a trade-off between enrichment and denaturation that was not detected by the statistical analysis. The influence of mixing conditions on recoverable activity is an important finding as it suggests that there are regimes in which one can operate where the recovered precipitate activity is the highest. The type of salt used in the precipitation may be critical; as the chaotropic nature of the precipitant increases, better mixing conditions will likely be required to avoid reductions in recoverable activity.

Our findings indicate that semi-batch precipitation operations should be run at high impeller speeds and low salt addition rates so that quick dilution of salt solutions can occur, reducing denaturing conditions and also possible nonspecific precipitation. However, the potentials for shear inactivation of protein, foaming and precipitate particle attrition place practical limits on agitation rates.

Theoretical results

The theoretical predictions for apparent solubility under various mixing conditions are in good agreement with the experimental results and are shown in Table 3. *No free parameters were used to fit the experimental results* as the constants in the mixing model were estimated independently. The solubility parameters β and K_S were obtained from Eq. 30. The values of the mixing parameters k_{ms} and k_{md} were estimated from the dye reaction experiments. The desolvation reaction rate constant, k_r, was estimated to be of the *order* of 50 s^{-1} based on kinetics studies of the salt-induced precipitation of α-chymotrypsin (Przybycien and Bailey, 1989a). A range of values for k_r was examined to determine the sensitivity of the model to this parameter.

Why does overprecipitation occur?

An examination of the salt environment in the points in the molecularly mixed zone provides insight into the discrepancy between apparent and theoretical solubilities. For our experimental conditions, in a type 1 point, the salt concentration increases from zero to its steady-state value of 1.5 M. Therefore, the thermodynamic solubility in such a point does not

ever go below P^*(1.5M) (see Figure 5). Hence, the type 1 points do not show any precipitation when the protein concentration is initial at or below the steady-state thermodynamic solubility.

Figure 5 also shows the corresponding type 2 point behavior during the course of a precipitation. In this simulation, the initial protein concentration is equal to the final thermodynamic protein solubility and, therefore, no reaction is expected to take place. However, in our reactor system, the concentrations of the protein and salt solutions contacting initially are double their final average concentrations and precipitation does take place. Due to the log-linear relationship between the protein solubility and the salt concentration as described by Eq. 28, the solubility in a given type 2 point, when the salt concentration is initially 3.0 M, is only 0.08 mg·mL^{-1} (see Figure 5 inset). Therefore, much of the protein that enters this point initially is desolvated. Since the precipitation is kinetically irreversible, redissolution of precipitate does not take place and a depressed solubility is observed.

Desolvation rate constant

The protein desolvation reaction rate constant, k_r, was varied in the simulations to predict its impact on the apparent solubility. Increasing values of k_r/k_{md} beyond 50 do not affect the apparent solubility as by this point, $k_r \gg k_{md}$ and the reaction is completely mixing controlled. When the value of k_r/k_{md} is between 0.01 and 10.0, there is a large effect on mass of protein precipitated and hence apparent solubility (see Figure 6a, top). At lower values of the dimensionless desolvation rate constant, when the reaction rate is controlling, the mass of protein precipitated is drastically reduced. The dependence of the apparent solubility on k_r indicates an avenue through which the salt type and protein type may exert an influence on apparent solubility. Salts which cause faster desolvation of the protein may require increased attention to management of mixing conditions during scale-up.

Cohn salting-out constant

The Cohn equation salting-out constant, K_S, was also varied to evaluate the impact of salt type on catalase apparent solubility. The simulations shown in Figure 6b (bottom) show mass of protein precipitated computed from Eq. 21. They indicate that under identical initial conditions, a protein-salt system having a higher K_S would precipitate to a greater extent. This behavior is fairly intuitive as higher salting out constants constitute a steeper solubility curve and consequently lower solubility at a given salt concentration for a given value of β. Differences in salting-out constants between two different proteins for a particular salt are routinely exploited in fractional precipitation; thus, the impact of mixing conditions on fractionation may be significant.

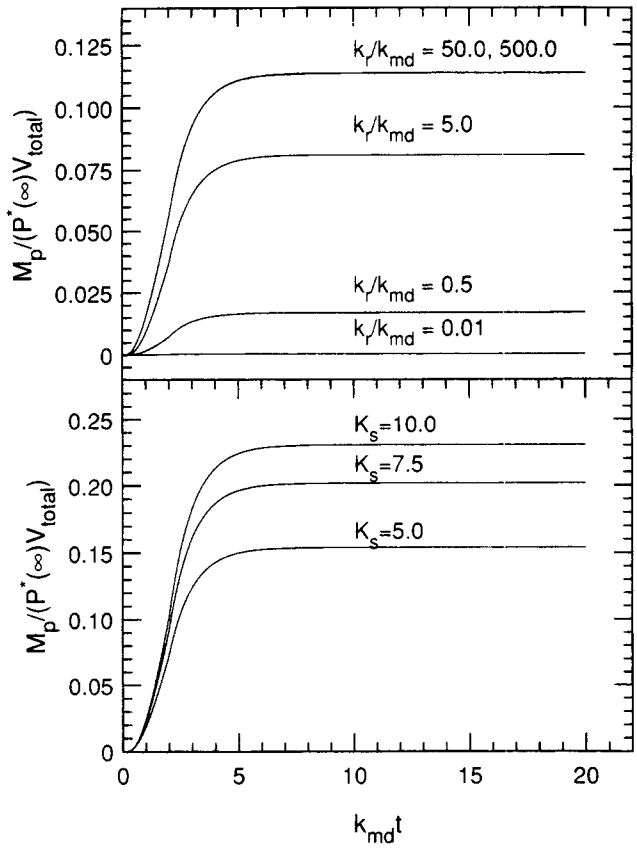

Figure 6. Plots showing mass of protein precipitated for (a, top) different reaction rate constants and (b, bottom) different salting-out constants.

Simulation conditions as in Figure 5.

Theoretical and experimental response surfaces

Using the statistical design analysis, theoretical and experimental response surfaces were obtained for apparent solubility predictions. The theoretical values of b_i are shown in Table 4. Figure 7a shows the experimental response surface at high initial protein concentration. Figures 7b and 7c show both the experimental and theoretical surfaces for the variation of apparent solubility with initial protein concentration, salt addition rate and impeller speeds derived from the theoretical and experimental b_i values. It can be seen that the experimental

Table 4. b_i Values from Statistical Analysis of Activity and Solubility Results

	b_1	b_2	b_3	b_{12}	b_{23}	b_{13}	b_{123}	b_o
b(exp.)solubility	0.56	4.25	−0.60	0.47	−0.62	−0.07	−0.06	6.24
b(theo.)solubility	0.0013	3.81	−0.0163	0.0013	−0.0163	0.0013	0.0013	5.75
b(exp.)activity	76.4	304.1	−53.1	139.6	−176.4	320.4	−66.4	1,507.4

X_1 = agitation speed (rpm); 60, 180, 540, X_2 = initial protein concentration (mg/mL); 4, 14.5, 25, X_3 = salt addition rate (ml/min); 8, 40, 200, Y = final protein solubility (mg/mL) or activity (U/mg). The (−1), (0) and (+1) entries represent low, moderate and high values of the manipulated variables, respectively. The b's are the coefficients used for generating the contours (b_i is the main effect, b_{ij} are the two-factor interactions and b_{ijk} is the three-factor interaction). The magnitude of b determines the extent of the effect. The sign of b shows if the effect is negative or positive. The final contour equation for the measured variable Y is (see Doehlert, 1985 for detailed explanations of this analysis): $Y = b_0 + b_1X_1 + b_2X_2 + b_3X_3 + b_{12}X_1X_2 + b_{13}X_1X_3 + b_{23}X_2X_3 + b_{123}X_1X_2X_3$.

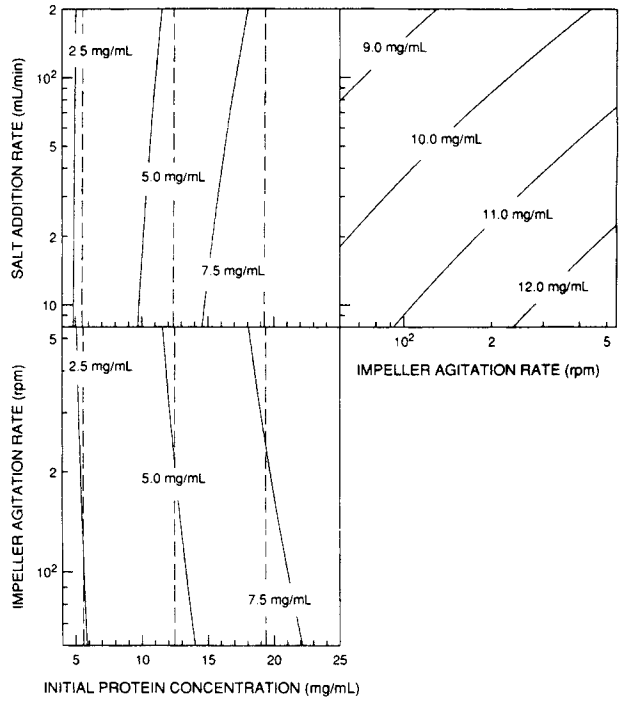

Figure 7. Experimental and theoretical response surfaces for apparent protein solubility.

(a, top right) impeller rate and salt addition rate at high initial protein concentration; (b, top left) salt addition rate and initial protein concentration at high impeller agitation rate; (c, bottom) impeller rate and initial protein concentration at high salt addition rate. Solid lines and dashed lines refer to experimental and theoretical contours, respectively.

effect of the initial protein concentration is tracked well by the theoretical surfaces as both theoretical and experimental b_2 values are in good agreement. Although both the theoretical and experimental surfaces show the same trends in apparent solubility, the theoretical surfaces underpredict the main effect of impeller speed and salt addition rate by an order of magnitude.

Scale-up considerations

Apparent solubility curves can be obtained for this system using the model simulations. Figure 8 gives apparent solubility curves as a function of initial protein concentration as well as physically meaningful mixing parameters and salt addition rates. Figure 8a (top) shows that the initial protein concentration emerges as an important scale-up parameter. Changes in the initial protein concentrations from 25 mg/mL to 5 mg/mL cause changes of the order of two orders of magnitude in the ultimate apparent solubility curve. All the curves show a slope towards the theoretical solubility and then drop rapidly once they approach the salting-out curve. There appears to be a slight drop in apparent solubility even at very low protein concentration. Keeping the initial concentration constant during scale-up should ensure that apparent solubilities will be the same order of magnitude as bench-scale experimental values.

Shih and coworkers (1992) performed small-scale (6 mL) precipitation experiments with α-chymotrypsin and proposed an explanation for the initial protein concentration dependence of the apparent protein solubility in terms of phase equilibrium

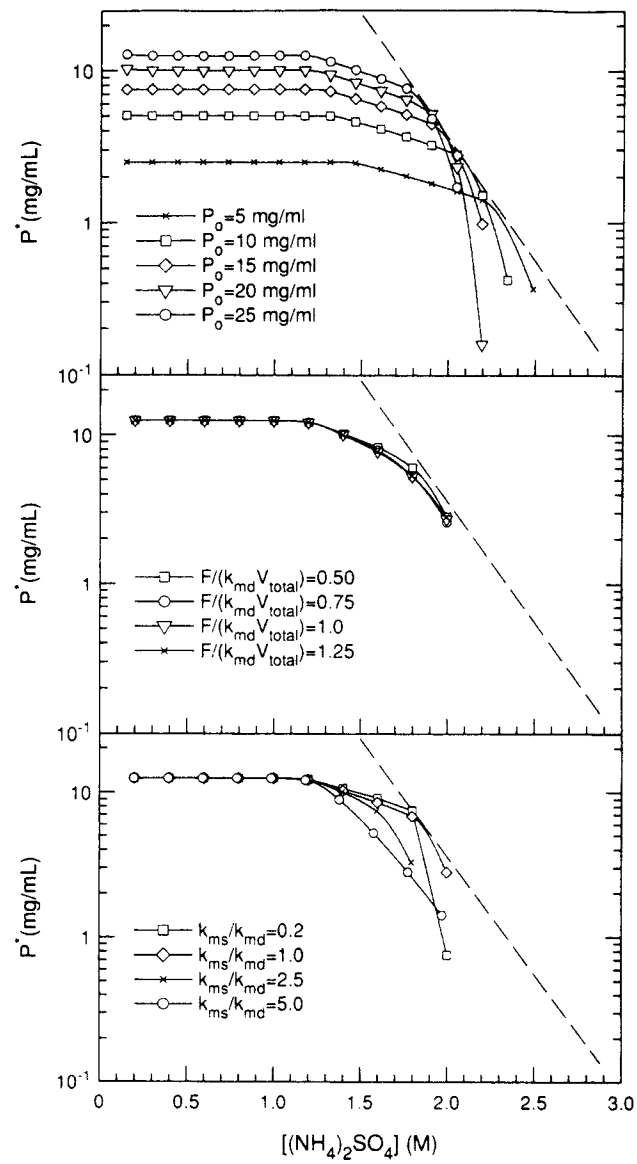

Figure 8. Apparent protein solubility curves.

(a, top) effect of initial protein concentration P_o with $F_s/V_{total}k_{md} = 0.25$ and $k_{md}/k_{ms} = 1.0$; (b, middle) effect of salt feed rate, $F_s/V_{total}k_{md}$ with $k_{md}/k_{ms} = 1.0$ and $P_o = 25$ mg/mL; and (c, bottom) effect of mixing conditions k_{md}/k_{ms} with $F_s/V_{total}k_{md} = 0.25$ and $P_o = 25$ mg/mL. The dashed line indicates thermodynamic solubility of crude catalase from Figure 3.

concepts. Our results, as interpreted through their theory, would indicate that changes in the observed solubility with respect to initial protein concentration and contacting conditions reflect the response of the solution phase to the composition of the precipitate phase in accordance with the phase distribution coefficient at the system temperature and pressure. Although both the initial protein concentration and the mixing conditions impact the precipitate phase composition, the circumstances under which precipitation can be viewed as an equilibrium process are not clear *a priori*. Indeed, prior small-scale work with a variety of salt-induced α-chymotrypsin precipitates indicated that only a fraction of each precipitate could be redissolved in neat buffer (Przybycien and Bailey, 1989). In the present work, catalase precipitations conducted at iden-

tical initial protein and salt concentrations, see Table 3 for $P_o = 25$ mg/mL, resulted in apparent solubilities that reflected the agitation and salt addition rates. Whether precipitation is a kinetically irreversible or equilibrium process depends on the relative rates of desolvation, aggregation and mixing; these phenomena. in turn, depend on the particular protein and salt as well as the geometry, scale and operating conditions of the precipitation vessel. At larger scales, we expect kinetic limitations to become increasingly apparent.

Figure 8b (middle) shows that apparent solubility is not impacted substantially by the salt feed rate. Figure 8c (bottom) shows that the mixing constants appear to affect the solubility substantially. When the micromixing is poor, $k_{ms}/k_{md} > 1.0$, the extent of overprecipitation is increased considerably due to persistently higher salt concentrations in the type 2 points. It can also be seen that when the micromixing is faster than the macromixing, $k_{ms}/k_{md} < 1.0$, overprecipitation becomes significant only at high salt concentrations. This is due to the fact that the precipitation reaction is assumed to take place only in the micromixed zone. Our model does not predict precipitation in the absence of agitation, or $k_{md} = 0$, but reality dictates that diffusion-driven surface precipitation does occur; one would expect the maximum overshoot in the apparent solubility at zero impeller speed. It must also be noted that, at larger scales, it becomes increasingly difficult to match power inputs per unit mass; as a result, k_{md} values become lower and k_r/k_{md} higher and therefore the extent of overprecipitation greater at larger scales as seen from the analysis above.

The dimensionless salt feed rate, $F_s/(V_{\text{total}}k_{md})$ is an indication of the ratio of rate of the salt addition to the rate at which salt is dissipated into the points by micromixing and represents another scale-up parameter. The value of $F_s/(V_{\text{total}}k_{md})$ would also have to be matched at higher scales. The value of k_{md} can be matched with a constant power input per unit mass of fluid in the reactor. The value of F_s cannot be scaled linearly indefinitely as it is physically impossible to have ever larger pumping rates for increasing reactor volumes. This parameter should impact solubility more significantly in larger-rather than smaller-scale systems. It is possible that we have looked at a range of $F_s/(V_{\text{total}}k_{md})$ values over which the solubility appears to be essentially invariant.

Conclusions

In protein precipitation processes, mixing conditions dictate observed protein solubilities. Of the process parameters examined in 1-L batch and semi-batch salting-out experiments, the initial protein concentration had the greatest impact on the extent of overprecipitation. The salt solution feed rate and agitation rate had much smaller effects. A decrease in initial protein concentration was found to decrease apparent protein solubility. Increased impeller speeds and decreased salt addition rates were found to improve mixing conditions and decrease the extent of overprecipitation. It is expected that the salt solution feed rate and the agitation rate will have greater significance at larger scales where extent of segregation is more significant. Suggested scale-up parameters for matching include the initial protein concentration and $F_s/(V_{\text{total}}k_{md})$.

The activity of recovered precipitates was found to vary substantially with differences in mixing conditions. At high salt addition rates and low impeller speeds, the activity was found to be depressed. This could be due to partial denaturation of protein due to harsh high salt environments under poor mixing conditions. Increasing impeller speeds caused quicker dilution of salt and increased recoverable activity. Fractionation of the crude mixture also caused an increase in the recovered activity due to enrichment of the precipitate. Understanding the impact of mixing on recoverable activity and fractionation behavior is crucial and has important ramifications for the recovery of expensive recombinant proteins through precipitation.

We have formulated a mixing model to describe protein overprecipitation phenomena. The model yields apparent solubility predictions that are in good qualitative agreement with the 1-L scale experimental observations. All model parameters were estimated from independent experiments. The correspondence between model predictions and experimental results suggests that our view of the physics of protein-precipitant contact and protein precipitation are consistent with reality; however, the robustness of the model with respect to scale remains to be examined.

The insights gained into apparent protein solubility have provided information about the underlying local supersaturation levels during precipitation. The local supersaturation will impact aggregate morphology via nucleation, perikinetic aggregation phenomena as well as fractionation behavior via differential thermodynamic solubilities and recoverable activity via irreversible aggregation. Our future work will address these issues as we continue to attempt to link precipitation process parameters to precipitate physical properties.

Acknowledgment

Funding for this research was provided by NSF Grant CTS-9211666.

Notation

A = 1-naphthol, M
A_λ = absorbance at wavelength λ
b_i = main effect of variable i in statistical analysis
b_{ij} = interaction of variables i and j in statistical analysis
$\underline{B}$ = diazonium salt of sulfanilic acid, M
C = average concentration of species C in molecularly mixed zone, mg/mL
C_f = concentration of species C in the bulk solution, M or mg/mL
C_i = concentration of species C in point i, M or mg/mL
D_t = diameter of precipitation reactor, mm
F_c = feed rate of component C, mL/min
H = Heaviside unit step function
k_1 = primary reaction rate constant in dye reaction, L/(mol·s)
k_2 = secondary reaction rate constant in dye reaction, L/(mol·s)
k_{md} = micromixing rate constant, 1/min
k_{ms} = macromixing rate constant, 1/min
k_r = protein desolvation rate constant, 1/s
K_s = Cohn equation salting-out constant, 1/M
l = path length of light beam through cuvette, cm
M_p = mass of protein precipitated, mg
P = protein concentration, mg/mL
P^* = protein solubility, mg/mL
P_o = initial protein concentration, mg·mL^{-1}
R = primary product of dye reaction, M
$\Re_c$ = reaction rate of species C, 1/(m·s)
S = secondary product of dye reaction, salt concentration, M
$\$$ = selectivity of dye reaction
t = time, s
V_c = segregated volume, mL
V_i = segregated volume of species i, mL
V_m = micromixed volume, mL
V_p = segregated volume of added protein solution, mL
V_{po} = initial segregated volume of added protein solution, mL

X_i = manipulated variables in statistical analysis
Y = observed variable in statistical analysis

Greek letters

β = Cohn equation constant for solubility of catalase in $(NH_4)_2SO_4$
ϵ = power input per unit mass, W/kg
ϵ_R = extinction coefficient for monoazo dyestuff, l(M·cm)
ϵ_S = extinction coefficient for bisazo dyestuff, l(M·cm)
λ = wavelength of light, nm
λ_K = Kolmogoroff velocity microscale, m
ν = kinematic viscosity, $m^5/(kg \cdot s)$
τ = time at which a point is formed, s

Literature Cited

Arakawa, T., and S. N. Timasheff, "Preferential Interactions of Proteins with Salts in Concentrated Solutions," *Biochem.*, **21**, 6545 (1982).

Arakawa, T., and S. N. Timasheff, "Abnormal Solubility Behavior of β-Lactoglobulin: Salting-In by Glycine and NaCl," *Biochem.*, **26**, 5147 (1987).

Baldyga, J., and J. R. Bourne, "Simplification of Micromixing Calculations: I. Derivation and Application of New Model," *Chem. Eng. J.*, **42**, 83 (1989).

Bell, D. J., M. Hoare, and P. Dunnill, "The Formation of Precipitates and Their Centrifugal Recovery," *Adv. Biochem. Eng.*, **26**, 1 (1983).

Bourne, J. R., F. Kozicki, and P. Rys, "Mixing and Fast Chemical Reaction: I. Test Reactions to Determine Segregation," *Chem. Eng. Sci.*, **36**, 1643 (1981).

Chan, M. Y. Y., M. Hoare, and P. Dunnill, "The Kinetics of Protein Precipitation by Different Reagents," *Biotechnol. Bioeng.*, **28**, 387 (1986).

Cohn, E. J., "The Solubility of Proteins," *Proteins, Amino Acids and Peptides*, E. J. Cohn and J. T. Edsall, eds., Chap. 23, Reinhold, New York (1943).

Costa, P., and C. Trevissoi, "Some Kinetic and Thermodynamic Features of Reactions between Partially Segregated Fluids," *Chem. Eng. Sci.*, **27**, 653 (1972).

Danckwerts, P. V., "The Effect of Mixing on Homogeneous Reactions," *Chem. Eng. Sci.*, **8**, 93 (1958).

Doehlert, D. H., *Experimental Strategies for Process Variables*, 4th ed., Edgework, Inc. (1989).

Drake, R. L., "A General Mathematical Survey of the Coagulation Equation," *Topics in Current Aerosol Research*, Vol. 3, Part 2, Hidy and Brock, eds., Pergamon Press, New York, p. 202 (1972).

Dunnill, P., "Trends in Downstream Processing of Proteins and Enzymes," *Process Biochem.*, **18**, 9 (1983).

Englard, S., and S. Seifter, "Precipitation Techniques," *Meth. Enzymol.*, **182**, 285 (1990).

Fisher, R. R., C. E. Glatz, and P. A. Murphy, "Effects of Mixing During Acid Addition on Fractionally Precipitated Protein," *Biotechnol. Bioeng.*, **28**, 1056 (1986).

Foster, P. R., P. Dunnill, and M. D. Lilly, "The Kinetics of Protein Salting-Out: Precipitation of Yeast Enzymes by Ammonium Sulfate," *Biotechnol. Bioeng.*, **28**, 545 (1976).

Fitchett, D. E., and J. M. Tarbell, "Effect of Mixing on the Precipitation of Barium Sulfate in a MSMPR Reactor," *AIChE J.*, **36**(4), 511 (1990).

Garside, J., and N. S. Tavare, "Mixing, Reaction and Precipitation: Limits of Micromixing in an MSMPR Crystallizer," *Chem. Eng. Sci.*, **40**(8), 1485 (1985).

Halicioglu, T., and O. Sinanoglu, "Solvent Effects on Cis-Trans Azobenzene Isomerisation: A Detailed Application of a Theory of Solvent Effects on Molecular Association," *Ann. N.Y. Acad. Sci.*, **158**, 308 (1969).

Hofmeister, F., "Zur Lehre von der Wirkung der Salze," *Arch. Exp. Path. Pharm.*, **24**, 247 (1887).

Hofmeister, F., "Uber die Darstellung von krystallisirtem Eiralbumin und die Krystallisirbarkeit colloider Stoffe," *Z. Physiol. Chem.*, **14**, 165 (1890).

Marcant, B., and R. David, "Experimental Evidence for and Prediction of Micromixing Effects in Precipitation," *AIChE J.*, **37**, 1698 (1991).

Melander, W., and C. Horvath, "Salt Effects on Hydrophobic Interactions in Precipitation and Chromatography of Proteins: An Interpretation of the Lyotropic Series," *Arch. Biochem. Biophys.*, **183**, 200 (1977).

Michaels, A., "Frontiers of Bioseparations Technology: Unsolved Problems and Novel Process Concepts," *Int. Conf. on Separations for Biotechnology*, Reading, UK pp. 3-8 (1990).

Nakayama, A., K. Kawamura, H. Shimada, A. Akaoka, I. Mita, M. Honjo, and Y. Furutani, "Extracellular Production of Human Growth Hormone by a Head Portion of the Prepropeptide Derived from *Bacillus Amyloliquefaciens* Neutral Protease in *Bacillus Subtilis*," *J. of Biotechnol.*, **5**, 171 (1987).

Nelson, C. D., and C. E. Glatz, "Primary Particle Formation in Protein Precipitation," *Biotechnol. Bioeng.*, **27**, 1434 (1985).

Niktari, M., S. Chard, P. Richardson, and M. Hoare, "The Monitoring and Control of Protein Purification and Recovery Processes," *Int. Conf. on Separations for Biotechnology*, Reading, UK, p. 622 (1990).

Paul, E. L., and C. B. Rosas, "Challenges for Chemical Engineers in the Pharmaceutical Industry," *Chem. Eng. Prog.*, 22 (Dec., 1990).

Petzold, L. R., "The DDASSL Differential/Algebraic System Solver," Sandia National Laboratory (1983).

Pohorecki, R., and J. Baldyga, "The Effects of Micromixing and the Manner of Reactor Feeding on Precipitation in Stirred Tank Reactors," *Ind. Eng. Chem. Fundam.*, **22**, 398 (1988).

Pohorecki, R., and J. Baldyga, "New Model of Micromixing in Chemical Reactors: 2. Application to a Stirred Tank Reactor," *Ind. Eng. Chem. Fundam.*, **22**, 398 (1983).

Przybycien, T. M., and J. E. Bailey, "Solubility-Activity Relationships in the Inorganic Salt Induced Precipitation of α-Chymotrypsin," *Enz. Microb. Technol.*, **11**, 264 (1989a).

Przybycien, T. M., and J. E. Bailey, "Aggregation Kinetics in Salt-Induced Protein Precipitation," *AIChE J.*, **35**, 1779 (1989b).

Przybycien, T. M., and J. E. Bailey, "Secondary Structure Perturbations in Salt-Induced Protein Precipitation," *Biochim. Biophys. Acta*, **1076**, 103 (1991).

Randolph, A. D., and M. Larson, *Theory of Particulate Processes*, Academic Press, New York (1971).

Reid, T. J., III, M. R. N. Murthy, A. Sicignano, N. Tanaka, W. D. L. Musick, and M. G. Grossman, "Structure and heme Environment of Beef Liver Catalase at 2.5 Å Resolution," *Proc. Natl. Acad. Sci., USA*, **78**(8), 4767 (1981).

Rice, R. W., and R. E. Baud, "The Role of Micromixing in the Scale-Up of Geometrically Similar Batch Reactors," *AIChE J.*, **36**(2), 293 (1990).

Righetti, G. P., and T. Caravaggio, "Isoelectric Points and Molecular Weights of Proteins," *J. Chromatogr. (Chromatographic Reviews)*, **127**, 1 (1976).

Rosensweig, R. E., "Idealized Theory for Turbulent Mixing in Vessels," *AIChE J.*, **10**, 91 (1964).

Rothstein, F., "Production Scale Issues in Protein Precipitation and Solid/Liquid Separation," *BioPharm Proc.*, Aster Publishing Corp., Eugene, OR (1991).

Scopes, R. K., *Protein Purification Principles and Practice*, Springer-Verlag, New York, p. 48 (1982).

Sedmak, J. J., and S. E. Grossberg, "A Rapid, Sensitive and Versatile Assay for Protein Using Coomassie Brilliant Blue G250," *Anal. Biochem.*, **79**, 544 (1977).

Shih, Ying-Chou, J. M. Prausnitz, and H. W. Blanch, "Some Characteristics of Protein Precipitation by Salts," *Biotechnol. Bioeng.*, **40**, 1155 (1992).

Sinanoglu, O., and S. Abdulnur, "Effect of Water and Other Solvents on the Structure of Biopolymers," *Fed. Proc.*, **24**, 12 (1965).

Tavare, N. S., and A. V. Patwardhan, "Agglomeration in a Continuous MSMPR Crystallizer," *AIChE J.*, **38**, 377 (1992).

Wistar, P., and P. D. Bartlett, "Kinetics of the Coupling of Diazonium Salts with Aromatic Amines in Buffer Solutions," *J. Amer. Chem. Soc.*, **63**, 413 (1941).

Wenger, K. S., E. H. Dunlop, and I. D. MacGilp, "Investigation of the Chemistry of a Diazo Micromixing Test Reaction," *AIChE J.*, **38**(7), 1105 (1992).

Åslund, B. L., and Å. C. Rasmuson, "Semibatch Crystallization of Benzoic Acid," *AIChE J.*, **38**(3), 328 (1992).

Manuscript received Jan. 12, 1993, and revision received June 10, 1993.